Biomaterials 192 (2019) 601–611

Contents lists available at ScienceDirect

Biomaterials

journal homepage: www.elsevier.com/locate/biomaterials

# An affinity-based approach to engineer laminin-presenting cell instructive microenvironments

Daniela Barros[a,b,c], Paula Parreira[a,b], Joana Furtado[a,d,1], Frederico Ferreira-da-Silva[a,d], Eduardo Conde-Sousa[a,b], Andrés J. García[e,f], M. Cristina L. Martins[a,b,c], Isabel Freitas Amaral[a,b,g,*], Ana Paula Pêgo[a,b,c,g,*]

[a] i3S - Instituto de Investigação e Inovação em Saúde, Universidade do Porto (UPorto), Portugal
[b] INEB - Instituto de Engenharia Biomédica, UPorto, Portugal
[c] ICBAS - Instituto de Ciências Biomédicas Abel Salazar, UPrto, Portugal
[d] IBMC - Instituto de Biologia Molecular e Cellular, UPorto, Portugal
[e] Parker H. Petit Institute for Bioengineering and Biosciences, Georgia Institute of Technology, Atlanta, GA, USA
[f] George W. Woodruff School of Mechanical Engineering, Georgia Institute of Technology, Atlanta, GA, USA
[g] FEUP - Faculdade de Engenharia, UPorto, Portugal

ARTICLE INFO

*Keywords:*
Laminin
Agrin
Affinity-binding
Protein immobilization
Self-assembled monolayers
Cell microenvironment

ABSTRACT

Laminin immobilization into diverse biological and synthetic matrices has been explored to replicate the microenvironment of stem cell niches and gain insight into the role of extracellular matrix (ECM) on stem cell behavior. However, the site-specific immobilization of this heterotrimeric glycoprotein and, consequently, control over its orientation and bioactivity has been a challenge that has limited many of the explored strategies to date. In this work, we established an affinity-based approach that takes advantage of the native high affinity interaction between laminin and the human N-terminal agrin (hNtA) domain. This interaction is expected to promote the site-selective immobilization of laminin to a specific substrate, while preserving the exposure of its key bioactive epitopes. Recombinant hNtA (rhNtA) domain was produced with high purity (> 90%) and successfully conjugated at its N-terminal with a thiol-terminated poly(ethylene glycol) (PEG) without affecting its affinity to laminin. Self-assembled monolayers (SAMs) of mono-PEGylated rhNtA on gold (mPEG rhNtA-SAMs) were then prepared to evaluate the effectiveness of this strategy. The site-specific immobilization of laminin onto mPEG rhNtA-SAMs was shown to better preserve protein bioactivity in comparison to laminin immobilized on SAMs of thiol-PEG-succinimidyl glutaramide (HS-PEG-SGA), used for the non-selective covalent immobilization of laminin, as evidenced by its enhanced ability to efficiently self-polymerize and mediate cell adhesion and spreading of human neural stem cells. These results highlight the potential of this novel strategy to be used as an alternative to the conventional immobilization approaches in a wide range of applications, including engineered coatings for neuroelectrodes and cell culture, as well as biofunctionalization of 3D matrices.

## 1. Introduction

In the framework of regenerative medicine and tissue engineering, much attention has been devoted towards the development of engineered matrices incorporating bioadhesive cues present in stem cell niches, to recapitulate the dynamic nature and biological complexity of these microenvironments, as well as gain more insight into the function of specific extracellular matrix (ECM) components on stem cell behavior. The ECM is an essential component of the stem cell niche, as it modulates important biological functions including proliferation, self-renewal and differentiation of stem cells. Among major ECM constituents, laminins play crucial and essential roles in many aspects of tissue physiology and function [1–5]. These heterotrimeric glycoproteins comprise several bioactive domains involved in the modulation of different biological functions. The latter include the interaction with other ECM proteins (*e.g.* nitrogen, netrin 4 and collagen VII) mediated by the laminin short arms (N-terminus), which contributes to the assembly and stability of basement membranes. These domains are also responsible for the laminin ability to polymerize [6–8], even in the absence of other basement membrane components, forming the

* Corresponding authors. i3S – Instituto de Investigação e Inovação em Saúde, Universidade do Porto, Rua Alfredo Allen, 208, 4200-135 Porto, Portugal.
*E-mail addresses:* iamaral@ineb.up.pt (I.F. Amaral), apego@i3s.up.pt (A.P. Pêgo).
[1] Current address: School of Life Sciences, Gibbet Hill Campus, The University of Warwick, Coventry, CVA4 7AL, UK.

https://doi.org/10.1016/j.biomaterials.2018.10.039
Received 18 July 2018; Received in revised form 14 October 2018; Accepted 28 October 2018
Available online 01 December 2018
0142-9612/ 

molecular network that will be in contact with the cellular surface. In addition to its structural role, laminin comprises multiple bioactive domains that interact with cell surface receptors (*e.g.* integrins, dystroglycans, and syndecans), modulating different cell functions including cell adhesion, proliferation, migration and differentiation, as well as ECM deposition [9–11].

Laminin has been incorporated into both two-dimensional (2D) [12] and three-dimensional (3D) [13–20] cell-instructive microenvironments for applications in regenerative therapies or to get insights into the role of laminin on the modulation of cell behavior. Strategies explored for laminin immobilization have relied either on its non-selective adsorption or entrapment or, alternatively, on its non-selective covalent immobilization to different substrates through the use of functional groups present in multiple sites of the laminin structure such as amines [13–17] and thiols [18,20]. One of the main caveats presented by these strategies is the inability to control orientation and conformation of laminin upon immobilization, which were proven to be crucial for the modulation of cellular behavior [21–23]. As such, the exposure of key laminin bioactive epitopes can be compromised. In an attempt to assure the control over the tethering of laminin, in recent years protein immobilization strategies have shifted toward site-specific conjugation, with special focus on biorthogonal chemical reactions (click chemistry), enzymatic ligation and affinity binding, using either unnatural amino acids or engineered site-selective amino acid sequences [24–26]. These strategies are expected to provide a higher retention of bioactivity, by favoring the access to the active sites of immobilized proteins. To the best of our knowledge, to date, only one study reported the site-selective immobilization of laminin [27]. To control the presentation of full-length ECM proteins without altering their bioactivity, Lee and co-workers explored click chemistry to anchor collagen, fibronectin and laminin onto polyacrylamide gels by their N-terminus [27]. Nevertheless, despite guaranteeing the site-selective immobilization of the proteins, as result of the use of laminin N-terminus, this approach compromises one of laminin's hallmark features, which is its ability to polymerize. Affinity-binding has been increasingly explored for the site-specific and reversible conjugation of proteins and peptides, because of its versatility and ability to generate dynamic biomimetic systems. However, the successful implementation of this strategy is strongly dependent on the appropriate selection of the binding pairs. Binding systems using high affinity interactions, such as streptavidin and biotin, although often used, require the protein of interest to be either recombinantly or chemically modified [28,29]. In contrast, the use of natural binding partners constitutes an attractive alternative, as strong non-covalent interactions can be achieved without the need for protein modification [30,31].

In this study, we examined an alternative strategy that explores the well described native high affinity interaction ($K_D$ = 5 nM) between laminin and the N-terminal agrin (NtA) domain [32,33]. The agrin-binding site in laminin is localized in the central region of its coiled-coil domain and maps to a sequence of 20 conserved residues within the γ1 chain [33,34]. Interestingly, this interaction requires a coiled-coil conformation of the agrin-binding site [34]. To assess the ability of this affinity-based approach to immobilize laminin with retention of bioactivity, recombinant human NtA (rhNtA) domain was successfully produced and further conjugated, at its N-terminus, with a thiol-terminated poly (ethylene glycol) (PEG) to enable the preparation of self-assembled monolayers (SAMs) of NtA on gold. To the best of our knowledge, this is the first report on the production and characterization of the human variant of NtA domain. In order to study the specific interactions between the immobilized laminin and cells, SAMs were herein used as proof-of-concept platforms, since they can be easily produced and specifically tailored to provide a chemically well-defined molecular monolayer [35]. The binding ligand was characterized and its ability to mediate laminin immobilization through a high affinity interaction was shown by solid-binding assay, surface plasmon resonance (SPR) and quartz crystal microbalance with dissipation monitoring (QCM-D). The bioactivity of mono-PEGylated rhNtA-immobilized laminin was subsequently investigated by evaluating its ability to self-polymerize and modulate the behavior of human neural stem cells (hNSCs). hNSCs were herein used due to the well described role of laminin on the modulation of neural cell behavior [36]. This strategy represents a promising and versatile approach for the site-selective immobilization of laminin while preserving its bioactivity, which can be potentially useful for the development of cell instructive microenvironments for tissue engineering and regenerative medicine.

## 2. Materials and methods

### 2.1. Recombinant human N-terminal agrin (rhNtA) domain expression and purification

The NtA domain, comprising residues Thr 30 – Pro 157 of the human agrin protein (Uniprot reference O00468), was expressed in *Escherichia coli* (*E. coli*) strain BL21 (DE3) using the pCoofy2 expression vector [37] (gift from Sabine Suppmann – Addgene plasmid # 43,981). pCoofy2 is a derivative of pETM22 vector that contains a thioredoxin-poly-$His_6$ (6x Histidine residues) (Trx-$His_6$) N-terminal tag followed by an HRV 3C recognition site located downstream of the N-terminal tag [37]. Details on cloning of human NtA gene and expression vector are presented in Supplementary Materials and Methods. The fusion protein (Trx-$His_6$-hNtA) was expressed by induction of log-phase cultures with 0.2 mM of isopropyl β-D-1-thiogalactopyranoside (IPTG; Sigma-Aldrich) at 20 °C for 5 h and purified by immobilized metal affinity chromatography using an HisTrap column (GE Healthcare), according to manufacturer's instructions. A concentration gradient of 0–500 mM of imidazole was applied to elute the fusion protein. The N-terminal Trx-$His_6$ tag was then cleaved during dialysis using HRV 3C protease (kindly provided by Biochemical and Biophysical Technologies (B2Tech) Platform of i3S) in a protease:target protein ratio (unit/μg) of 1:10. Untagged recombinant human NtA (rhNtA) contains additional Gly and Pro residues at its N-terminus (Fig. S1). rhNtA was dialyzed against 10 mM phosphate buffered saline (PBS) pH 7.4, concentrated in a 10 kDa molecular weight cut-off (MWCO) ultrafiltration membrane (GE Healthcare) and stored at −80 °C until further use. Final domain concentration was estimated by measuring the absorbance at 280 nm. The purity of the rhNtA domain was assessed by sodium dodecyl sulfate–-polyacrylamide gel electrophoresis (SDS-PAGE) analysis and Western blotting using the *anti*-agrin antibody - rabbit polyclonal agrin antibody (1:5000; Abcam, ab85174). The rhNtA molecular weight was determined by mass spectrometry, as described in section 2.7.

### 2.2. Solid-phase binding assay

Binding of rhNtA to immobilized laminin was assessed performing an enzyme-linked binding assay (ELISA). 96-well microtiter ELISA plates (BD Falcon) were coated with poly (D-lysine) (PDL; 20 μg/mL; Sigma-Aldrich) and then incubated with laminin-111 from mouse Engelbreth-Holm-Swarm sarcoma (msLn-111; 10 μg/mL; Sigma-Aldrich) in 50 mM sodium bicarbonate buffer pH 9.6 (overnight, 4 °C). After blocking with 2.5% (w/v) bovine serum albumin (BSA; Biowest; 1.5 h, room temperature (RT)), wells were incubated with 2-fold serial dilutions of rhNtA (0.1–100 nM; 2 h, 37 °C). Plates were then washed with PBS/0.05% (v/v) Tween® 20 and incubated with rabbit polyclonal agrin antibody (1:5000; 2 h, RT). A goat anti-rabbit IgG (H + L) coupled to horseradish peroxidase (HRP) (1:2000; Life Technologies, A16023) was used as secondary antibody, and color was developed using 3,3′,5,5′ tetramethyl benzidine (TMB) as substrate (Biolegend; 30 min, RT). The reaction was stopped with 2 M $H_2SO_4$ and the absorbance measured at 450 nm (BioTek® Synergy™ Mx). The dissociation constant ($K_D$) value of rhNtA to msLn-111 was estimated by non-linear regression analysis using GraphPad Prism 6 software (San Diego).

### 2.3. Surface plasmon resonance (SPR)

Real-time interactions between rhNtA and immobilized laminin were detected by SPR at 25 °C using a BIACORE X100 (GE Healthcare). Laminin was immobilized on a CM5 sensor chip (GE Healthcare) using amine-coupling chemistry. Briefly, the flow cells surface was activated with a 1:1 mixture of 0.1 M N-hydroxysuccinimide (NHS; Sigma-Aldrich) and 0.4 M 3-(N,N-dimethylamino) propyl-N-ethylcarbodiimide (EDC; Sigma-Aldrich) at a flow rate of 10 μL/min msLn-111 or recombinant human laminin-521 (rhLn-521; Biolamina) (50 μg/mL in 10 mM sodium acetate pH 3.5) were immobilized at a density of 4000 resonance units. The reactive groups in excess were then deactivated with 1 M ethanolamine-HCl pH 8.5 (Sigma-Aldrich). For binding measurements, 5-fold serial dilutions of rhNtA (500–0.8 nM) were prepared in 10 mM 4-(2-hydroxyethyl)-1-piperazineethanesulfonic acid (HEPES; pH 7.4, containing 150 mM sodium chloride (NaCl; VWR), 3 mM Ethylenediamine tetra-acetic acid (Sigma-Aldrich) and 0.005% (v/v) surfactant P20 (GE Healthcare)) and flowed at 30 μL/min onto the flow cells. Proteins were allowed to associate and dissociate for 120 and 1600 s, respectively. Experimental results were fitted with Langmuir 1:1 binding kinetics within Biacore X100 Evaluation software version 2.0.1 (GE Healthcare).

### 2.4. Culture of H9 – derived human neural stem cells

Human neural stem cells (hNSCs) derived from the National Institutes of Health (NIH) approved H9 (WA09) human embryonic stem cells were purchased from Life Technologies (N7800-200). Cells were expanded according to the manufacturer's protocol in poly (ornithine)/msLn-111-coated tissue culture-treated plates in serum-free StemPro® NSC SFM growth medium (Life Technologies).

### 2.5. Cell adhesion centrifugation assay

To evaluate the ability of rhNtA-immobilized msLn-111 to promote the adhesion of hNSCs, a centrifugation cell adhesion assay was performed [38]. Here, controllable and reproducible detachment forces were applied to adherent cells, providing relative measurements of adhesion strength [38]. 96-well tissue culture plates (Corning) were coated with increased concentrations of rhNtA (0–40 μg/mL) overnight at 4 °C and blocked with 1% (w/v) BSA for 1 h at RT to prevent non-specific adhesion to the substrate. msLn-111 was then added at a fixed concentration (10 μg/mL), the plate incubated for 2 h at 37 °C and hNSC adhesion assessed as described in Supplementary Materials and Methods. Wells incubated with 1% (w/v) BSA or 20 μg/mL poly (ornithine)/10 μg/mL msLn-111 were used as negative and positive control, respectively. To assess the effect of the domain *per se* on cell adhesion, wells incubated with 10 μg/mL rhNtA were used.

### 2.6. N-terminal PEGylation of rhNtA

A 5 mg/mL rhNtA solution in 0.1 M sodium phosphate ($NaH_2PO_4$) pH 6.5 was added to thiol-PEG-succinimidyl glutaramide (HS-PEG-SGA; 3.5 kDa; purity > 90%, Jenkem USA) at a protein:PEG molar ratio of 1:2. The reaction was allowed to proceed for 4 h at 4 °C and then quenched with 2 M hydroxylamine pH 7.4. The solution was diluted to a final protein concentration of 0.5 mg/mL with 1 mM HCl and the pH adjusted to 3.5 with 1 M HCl. The reaction mixture was then diluted (100 × ) with 20 mM sodium acetate pH 4.0 and loaded onto a HiTrap SP HP cation exchange column (GE Healthcare). A gradient of 0–1 M NaCl in 20 mM sodium acetate pH 4.0 was used to elute the different PEGylated fractions. The peak corresponding to the mono-N-terminal conjugate was dialyzed against 10 mM PBS pH 7.4, concentrated in a 10 kDa MWCO ultrafiltration membrane (GE Healthcare) and stored at −80 °C until further use. Protein concentration was estimated by measuring the absorbance at 280 nm and the conjugate was characterized by SDS-PAGE and MALDI-TOF mass spectrometry (MALDI-TOF MS).

### 2.7. Protein and PEGylated conjugate characterization by mass spectrometry

The native or mono-PEGylated rhNtA, as well as unmodified HS-PEG-SGA, were analyzed by MALDI-TOF MS. Briefly, samples were diluted 1:4 (v/v) in MALDI matrix (sinapinic acid 10 mg/mL, 50% acetonitrile, 0.1% trifluoroacetic acid, all purchased from Sigma-Aldrich), spotted onto a target plate and analyzed in linear positive mode. Mass spectra were internally calibrated with thioredoxin (*m/z* 11,674) and apomyoglobin (*m/z* 16,952). To characterize the site of PEG conjugation to rhNtA, peptide mapping of native and mono-PEGylated rhNtA was performed using a previously published procedure [39], which is briefly described in Supplementary Materials and Methods.

### 2.8. Self-assembled monolayers (SAMs) preparation

Mixed SAMs of mono-PEGylated rhNtA (mPEG rhNtA-SAM) or HS-PEG-SGA (SGA-SAM) were prepared on gold-coated substrates (0.5 × 0.5 $cm^2$), obtained from Instituto de Engenharia de Sistemas e Computadores – Microsistemas e Nanotecnologias, Portugal (INESC-MN). Prior to use, gold surfaces were cleaned as described elsewhere [40]. Gold substrates were then incubated in ethanolic solutions (99.9%; Merck-Millipore) of either mono-PEGylated rhNtA (2.5, 5.0 or 10.0 μM), for laminin affinity binding; or HS-PEG-SGA (5.0 μM), for non-selective covalent immobilization of laminin. After 4 h at RT and under inert conditions (glove chamber saturated with dry nitrogen), SAMs were rinsed with absolute ethanol to remove any physically adsorbed molecules. For proper monolayer packing mPEG rhNtA- and SGA- SAMs were subsequently incubated with a 100.0 μM absolute ethanolic solution of (11-mercaptoundecyl) tetraethylene glycol (EG4, SensoPath Technologies) for 16 h at RT and under the inert conditions mentioned above. Afterwards, SAMs were thoroughly rinsed with absolute ethanol (99.9%; Merck-Millipore). EG4-SAMs, used as control surfaces, were prepared by immersing cleaned gold substrates in a 100.0 μM ethanolic solution of EG4 for 16 h at RT and under inert conditions.

### 2.9. Quartz crystal microbalance with dissipation monitoring (QCM-D)

Gold-coated QCM-D sensors (Biolin Scientific) were cleaned as previously described [41]. Clean sensors were further modified following the procedure reported in 2.8. A QCM-D system (Q-Sense E4 instrument, Biolin Scientific) was used to monitor in real time the frequency (Δf) and dissipation (ΔD) shifts related to laminin adsorption as described in Supplementary Materials and Methods. Data was modeled using the Voigt model [41] in the QTools® V3 software. Results are presented as mass per surface area (ng/$cm^2$).

### 2.10. Laminin self-polymerization

mPEG rhNtA-SAMs were equilibrated in 10 mM HEPES pH 7.4, to favor the affinity interaction with laminin, while SGA-SAMs were equilibrated in 100 mM sodium bicarbonate pH 8.5, to favor the non-selective covalent interaction with laminin amine groups, and then incubated with msLn-111 (20 μg/mL; 2 h, RT). The substrates were then thoroughly washed, to remove any unbound laminin. To assess the ability of laminin to self-polymerize, a msLn-111 solution (50 μg/mL) in 20 mM Tris-HCl pH 7.0, containing 1 mM $CaCl_2$, was used. The laminin concentration used was below the critical protein concentration necessary to trigger laminin polymerization in neutral pH solution [6]. Mixed SAMs with affinity- (mPEG rhNtA-SAMs) or covalent-bound (SGA-SAMs) msLn-111 were incubated with the laminin solution for

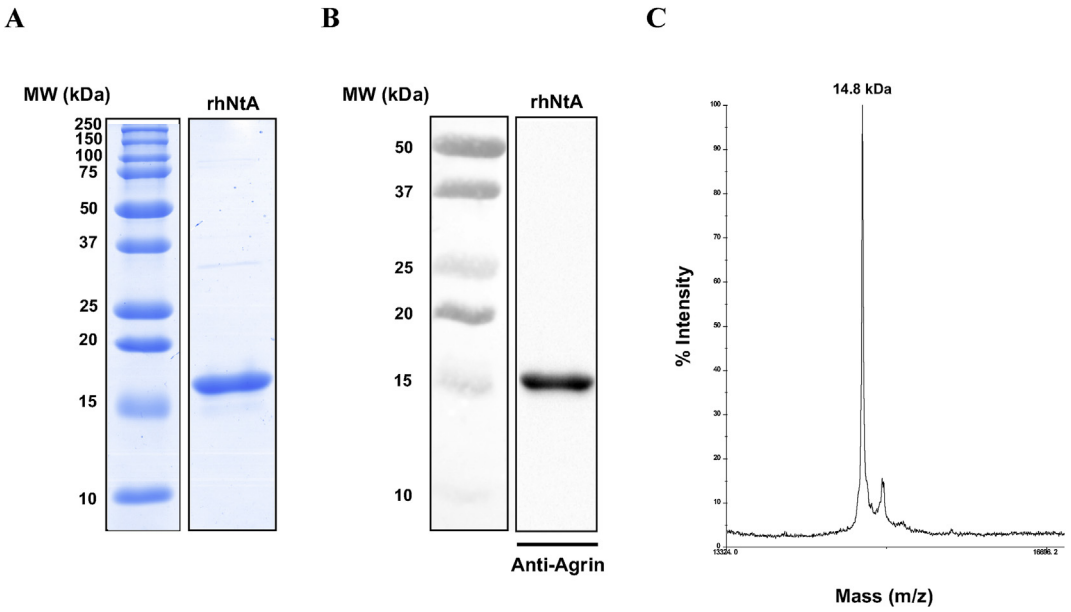


**Fig. 1. Recombinant human NtA (rhNtA) domain characterization. A)** Coomassie Blue stained 15% SDS-PAGE gel and **B)** Western-blot analysis of 10 µg of purified rhNtA. MW, Molecular Weight marker. **C)** MALDI-TOF MS spectra of purified rhNtA.

24 h at 37 °C [42]. Finally, samples were processed for laminin immunostaining, as described in Supplementary Materials and Methods, and observed under confocal laser scanning microscopy (CLSM) (TCS SP5 II; Leica Mycrosystems), using a Plan-Apochromat 63 × /1.4NA oil objective. A z-section of 15 µm was acquired and subsequently projected into a 2D image. Processing and quantitative analysis of the acquired images were performed in ImageJ/Fiji and MATLAB® software, respectively, as described in detail in the Supplementary Materials and Methods.

### 2.11. Cell adhesion and morphology

To determine the impact of the immobilization approach on the cell adhesion-promoting activity of laminin, mPEG rhNtA- or SGA-SAMs were equilibrated in 10 mM HEPES pH 7.4 and then incubated for 2 h at RT with rhLn-521 (20 µg/mL). After being washed with 10 mM HEPES pH 7.4 to remove unbound laminin, hNSCs (50,000 viable cells/cm$^2$) were added to the substrates and incubated at 37 °C with 5% $CO_2$ for 24 h. Samples were processed for F-actin/DNA staining, as described in Supplementary Materials and Methods, and imaged with the IN Cell Analyzer 2000 imaging system (GE Healthcare) using a Nikon 20 × / 0.45 NA Plan Fluor objective. A z-section of 45 µm was acquired per field of view (FOV) and then projected into a 2D image. Images spanning a total area of 4.6 mm$^2$ were analyzed using CellProfiler image analysis software [43]. Briefly, nuclei were segmented through an Otsu thresholding method from the 4',6-diamidino-2-phenylindole (DAPI) channel while cells cytoplasm was segmented from the actin channel through a propagation from the previously identified nucleus, using a minimum cross entropy threshold. Measurements were obtained for total number of adhered cells, average cell spreading area (µm$^2$) and average occupied area (µm$^2$) per FOV. Representative images for each condition were also obtained by CLSM using a Plan-Apochromat 63 × / 1.4NA oil objective. A z-section of 12 µm was acquired and subsequently projected into a 2D image.

### 2.12. Statistical analyses

Individual experiments with biological replicates were performed at least in duplicate and statistical analysis was performed using GraphPad Prism 6 software (San Diego). Statistically significant differences between two conditions were detected using a non-parametric Mann Whitney *U* test. Comparisons between three or more groups were performed with one-way ANOVA analysis, followed by the Bonferroni correction for pairwise comparisons or the Dunnett's two-tailed test for comparisons with the control condition. For all analyses, differences were considered significant at $p < 0.05$.

## 3. Results and discussion

### 3.1. Recombinant human N-terminal agrin (rhNtA) domain was successfully produced

In contrast with most of reports published to date in which the NtA used was derived from chicken agrin [32,33], we produced the human variant of this domain because of its higher clinical relevance. This is of particular interest when envisaging the use of this domain in platforms for human-disease modelling, cell culture/delivery or engineered coatings for neuroelectrodes.

The produced fusion protein Trx-His$_6$-hNtA, revealed high affinity binding to msLn-111 with an equilibrium dissociation constant ($K_D$) of 6.49 ± 0.58 nM, as determined by solid-phase binding assay (Fig. S2), similar to that reported for chicken NtA - msLn-111 interaction ($K_D$ = 5 nM) [32,33]. Cleavage of the N-terminal tag was subsequently conducted to enable conjugation of a thiol-terminated PEG moiety to the domain N-terminal, for further immobilization of rhNtA to the selected substrate. This immobilization approach was chosen to assure the exposure of the high-affinity laminin binding site of rhNtA, located on the C-terminal [32,44]. Untagged rhNtA domain was produced with a high purity (> 90%) and with the expected MW 14.5 kDa, as evidenced by Coomassie blue staining (Fig. 1A) and Western blot analysis (Fig. 1B). Molecular weight was further confirmed by MALDI-TOF MS (MW 14.8 kDa) (Fig. 1C).

rhNtA was shown to mediate a high affinity interaction with msLn-111 ($K_D$ = 5.85 ± 0.43 nM), as evidenced by solid-phase binding assay (Fig. 2). To monitor in real time the interaction between rhNtA and immobilized msLn-111 or rhLn-521, SPR was conducted (Table 1). Native rhNtA was found to interact with high affinity with both msLn-111 and rhLn-521 ($K_D$ = 0.98 ± 0.02 and 0.54 ± 0.14 nM, respectively; Table 1), showing that binding affinity towards laminin was retained independently of the laminin isoform. Results from both

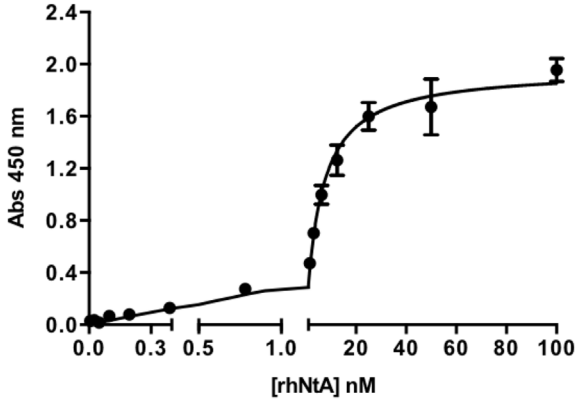


**Fig. 2. rhNtA Bioactivity**. Solid-phase assay of rhNtA binding to immobilized msLn-111 (10 μg/mL). The results are shown as fitted curve of the mean ± standard deviation (SD) of three replicate samples from one experiment representative of three independent assays. Non-linear regression analysis revealed a $K_D$ value of rhNtA to msLn-111 of 5.85 ± 0.43 nM ($r^2 = 0.99$).

**Table 1**
Kinetic parameters ($k_a$, association rate constant; $k_d$, dissociation rate constant) and affinity constant ($K_D$, dissociation constant) of rhNtA to immobilized msLn-111 or rhLn-521, estimated by SPR. Data represent mean ± SD of three independent experiments.

| | $k_a$ (x$10^5$) $M^{-1}.s^{-1}$ | $k_d$ (x$10^{-4}$) $s^{-1}$ | $K_D$ (nM) |
|---|---|---|---|
| **msLn-111** | 5.25 ± 1.83 | 5.12 ± 1.71 | 0.98 ± 0.02 |
| **rhLn-521** | 4.86 ± 1.55 | 2.52 ± 0.43 | 0.54 ± 0.14 |

techniques indicate that the laminin binding site of the produced rhNtA domain preserved its bioactivity, namely the ability to interact with high affinity with laminin.

### *3.2. rhNtA-immobilized laminin is able to mediate cell adhesion of human neural stem cells*

Laminin mediates integrin- and non-integrin-dependent adhesion of neural stem cell (NSCs) [45–47], being commonly used as a surface coating for NSC culture. As the site-specific immobilization of laminin should preserve exposure of its multiple bioactive domains interacting with cell adhesion receptors and, therefore, its cell adhesion-promoting activity, we assessed the ability of rhNtA-immobilized msLn-111 to mediate cell adhesion of hNSCs. These cells were seeded on cell culture wells coated with rhNtA-immobilized msLn-111 and cell adhesion quantified, as a function of rhNtA concentration, using a centrifugation adhesion assay [38] (Fig. 3). The application of a constant centrifugal force revealed an increase in cell adhesion with the increase of the rhNtA concentration from 0.1 to 10 μg/mL (Fig. 3), at which the levels of cell adhesion observed on rhNtA-immobilized msLn-111 reached values similar to those on the msLn-111 positive control (Fig. 3). This suggests that under these conditions, the amount of affinity-immobilized msLn-111 attained a plateau, which is in agreement with the isotherm of rhNtA adsorption (Fig. S3) that shows a saturation plateau at domain concentrations ≥ 2.5 μg/mL. The cell adhesion levels observed in the absence of rhNtA (0 μg/mL rhNtA) are most likely due to the competitive displacement of adsorbed BSA by laminin, an effect also known as the Vroman effect [48]. Cell adhesion to wells incubated only with rhNtA (10 μg/mL) was, as expected, comparable to that observed on the negative control (BSA; Fig. 3), due to the absence in the rhNtA of bioactive cell adhesion domains. These results demonstrate that, when immobilized through rhNtA, laminin retains its ability to mediate cell adhesion, suggesting the correct exposure of laminin's main bioactive sites interacting with cell surface receptors.

### *3.3. rhNtA is selectively PEGylated at the N-terminus*

The rhNtA sequence comprises seven primary amines, including the α-amine of Gly1 and the ε-amine of six Lys residues (Fig. S1), which can theoretically react with the SGA group in HS-PEG-SGA. The site-specific addition of the PEG moiety at the N-terminal domain (α-amine) of rhNtA can be controlled by adjusting the pH at which the PEGylation reaction occurs and by adjusting the protein:PEG molar ratio. The conjugation reaction was performed at pH 6.5 and using a protein:PEG molar ratio of 1:2. The slightly acidic pH directs the PEGylation reaction to the α-amino group at the N-terminal of rhNtA, by taking advantage of the differences in pKa values of the α-amino group (pKa 7.8) [49,50] *versus* that of the ε-amino groups (pKa 10.1) [49,50] on the side chains of Lys residues. These conditions favor the protonation of the ε-amino groups of Lys, while assuring the availability of the α-amino group at the N-terminal as nucleophile. The cation-exchange chromatogram of the conjugation mixture (Fig. 4A) showed three different fractions, which correspond, as evidenced by molecular weight estimation from SDS-PAGE analysis (Fig. 4B), to rhNtA PEG conjugates containing either a double (MW ≅ 36.5 kDa; di-PEGylated rhNtA, peak 1) or single (MW ≅ 28.8 kDa; mono-PEGylated rhNtA, peak 2) PEG molecule and native rhNtA (MW ≅ 14.5 kDa, peak 3). The efficiency of the PEGylation reaction was determined based on the SDS-PAGE analysis (Fig. 4B). A PEGylation yield of 47% was obtained, from which 94% corresponds to mono-PEGylated rhNtA and the remaining 6% to di-PEGylated rhNtA. Since the large hydrodynamic volume of PEGylated proteins retards their mobility on SDS-PAGE gels, resulting in higher molecular weight estimates [49], PEGylation reaction products were further analyzed by MALDI-TOF MS for an absolute estimation of their molecular weight. The MALDI-TOF MS spectra of native and PEGylated rhNtA (Fig. 4C) indicate a molecular weight centered at 18.4 and 22.1 kDa for mono- and di-PEGylated rhNtA, respectively (the MW of native rhNtA was found to be 14.8 kDa, confirming the previously determined value (Fig. 1C)).

The position of the conjugated PEG moiety on the purified mono-PEGylated rhNtA conjugate was further determined by peptide mapping, comparing the fingerprint of native- and PEGylated rhNtA. The majority of the theoretical fragments, as well as the rhNtA N-terminus were experimentally detected in both samples (Table S2). Also, their molecular masses, which were experimentally determined by MALDI-TOF MS, are very similar to the predicted values obtained in *web.expasy.org/peptide_mass* (Table S2). Two peaks corresponding to the N-terminus of rhNtA domain were identified in both native and mono-PEGylated rhNtA – GPTCPER (F1) 1–7 *m/z* 816.3677 (Table S2, Fig. S4A) and GPTCPERALER (F2) *m/z* 1285.6278 (Table S2, Fig. S4B). In the conjugated sample, a significant decrease in the signal-to-noise ratio was observed for F1, while the peak correspondent to F2 was not detected. These evidences demonstrate that the α-amine of Gly1 was selectively modified with the PEG moiety.

### *3.4. N-terminal PEGylated rhNtA binds with high affinity to laminin*

SPR analysis was conducted to evaluate the impact of N-terminal PEGylation on rhNtA laminin binding ability. N-terminal PEGylation led to a decrease of the binding affinity for both msLn-111 ($K_D$ = 3.36 ± 0.11 nM) and rhLn-521 ($K_D$ = 1.58 ± 0.41 nM) (Table 2), estimated as a 3.4- and 2.9- fold decrease, respectively, compared to native rhNtA (Table 1). This suggests that PEG conjugation to rhNtA slowed down the rate of domain association ($k_a$) towards immobilized laminin, while the dissociation rate ($k_d$) was not affected (Table 2). Interestingly, the affinity of both native (Table 1) and mono-PEGylated rhNtA (Table 2) for rhLn-521 was found to be slightly higher than that determined for msLn-111. Moreover, the complex formed with this laminin isoform appears to be more stable, as evidenced by higher $k_d$ values (Tables 1 and 2). Previous studies suggest that the affinity between NtA and laminin is regulated by laminin chain

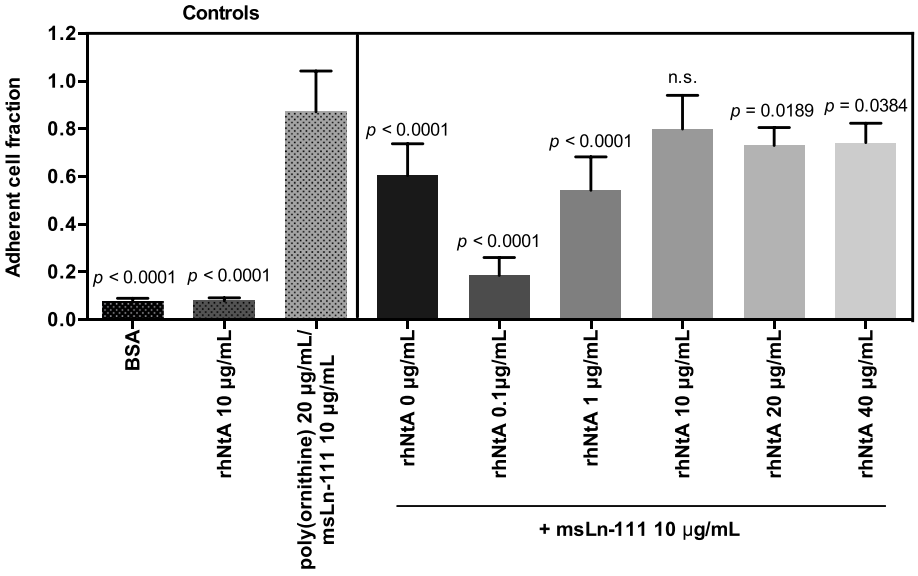


**Fig. 3.** hNSC adhesion to rhNtA-immobilized msLn-111 (10 µg/mL) as a function of rhNtA concentration (0.1–40 µg/mL), evaluated performing a cell adhesion centrifugation assay. The number of adherent cells on wells coated with BSA (1% (w/v), negative control), rhNtA (10 µg/mL) and 20 µg/mL poly (ornithine)/10 µg/mL msLn-111 (positive control), is also shown. Data represent mean ± SD of 10–18 replicates from two independent experiments; one-way ANOVA followed by Dunnett's test (*vs.* poly (ornithine)/msLn-111).

composition, and that although the agrin binding site is located within the γ1 chain, α and β laminin chains may also contribute to the binding, even though to a lesser extent [32,33,51]. Therefore, the differences observed in the binding affinity of native and mono-PEGylated rhNtA to msLn-111 and rhLn-521 can be related to the chain composition of the laminin isoforms tested.

### 3.5. N-terminal PEGylated rhNtA can be used for the site-selective immobilization of laminin with retention of bioactivity

The potential of mono-PEGylated rhNtA to promote the site-selective immobilization of laminin onto substrates was explored using mixed SAMs of mono-PEGylated rhNtA and (11-mercaptoundecyl) tetraethylene glycol (EG4) (mPEG rhNtA-SAMs) as a model surface. EG4 was used to prevent nonspecific protein immobilization and thus guarantee signal specificity and maximum bioactivity of the immobilized biomolecules, while also enhancing the correct monolayer packing [52]. Mixed SAMs of HS-PEG-SGA and EG4 (SGA-SAMs) were also prepared to promote the non-selective covalent immobilization of laminin through the reaction with protein amine groups present in multiple locations within the laminin structure.

To avoid steric effects and have a finer control over the binding ligand surface density, which ultimately would determine the amount of affinity-bound laminin, an initial screening was conducted to determine the most suitable mono-PEGylated rhNtA domain concentration. QCM-D analysis was conducted with different mono-PEGylated rhNtA concentrations (2.5, 5.0 and 10.0 µM) while keeping that of EG4 constant (100.0 µM), to evaluate laminin immobilization (Fig. S5). Results show a more effective laminin immobilization when an intermediate concentration of mono-PEGylated rhNtA (5.0 µM) was used (638 ± 29 ng/cm$^2$, compared to the 146 ± 115 and 445 ± 57 ng/cm$^2$, obtained for 2.5 and 10.0 µM mono-PEGylated rhNtA, respectively) (Fig. S5). Based on these results, mixed SAMs were prepared using an intermediate concentration (5.0 µM) of either mono-PEGylated rhNtA or HS-PEG-SGA.

Infrared reflection absorption spectroscopy (IRRAS) analysis was performed to characterize the prepared mixed mPEG rhNtA- and SGA-SAMs, using Au surfaces as background. EG4-SAMs and adsorbed native rhNtA to Au surfaces were used as controls. The presence of rhNtA domain was confirmed by the detection of the two protein characteristic absorption bands correspondent to amide I (1690 ± 45 cm$^{-1}$), which is mainly associated with C═O stretching vibration and is directly related to the backbone conformation, and amide II (1540 ± 60 cm$^{-1}$), which results from the N−H and C−N vibration that were observed on both native rhNtA and mPEG rhNtA spectra (Fig. S6). An absorption band at 1690 cm$^{-1}$ was also observed in the PEG-SGA spectrum, which is attributed to the C═O stretching vibration from the SGA group.

#### 3.5.1. Site-selective immobilized laminin retains its ability to self-polymerize

Laminin polymerization is a key process to direct basement membrane assembly and organization and occurs by a thermally reversible process dependent on the presence of calcium ions [6–8]. Previous studies exploring this hallmark feature of laminin demonstrated that this ECM protein is able to spontaneously self-polymerize in solution at neutral pH, requiring a minimal protein concentration of approximately 60 nM [6]. The three-arm interaction model has been proposed by Cheng and co-workers (Fig. 5A) to explain the mechanism of laminin polymerization. This model proposes that the three laminin N-terminal short arms are able to interact with the globular N-terminal domains of other laminins to form a polygonal network, contributing to the basement membrane architecture [6–8,53]. The long arm of the laminin heterotrimer, in turn, is predicted not to be involved in the network formation, being free to interact with cells out of the plan of the polymer. Based on this evidence, we evaluated the ability of laminin to self-polymerize when immobilized onto mPEG rhNtA-SAMs (Fig. 5B, left panel) or SGA-SAMs (Fig. 5B, right panel). Differences between the two conditions were assessed by image processing and quantitative analysis, using ImageJ/Fiji and MATLAB® software, respectively. Four different variables were measured, including number of aggregates (Fig. 5C), aggregate average size (Fig. 5D), perimeter (Fig. 5E) and maximum Feret's diameter (Fig. 5F). More information about the specific meaning of each measured variable can be found in https://imagej.nih.gov/ij/docs/menus/analyze.html. The relationship among the number of aggregates, aggregate average size, and perimeter provides information on laminin's ability to form larger organized polygonal-shape structures *versus* several small unstructured aggregates, whereas the maximum Feret's diameter provides a good indicator of network organization. An organized polygonal network consisting mainly of lamellar aggregates was consistently observed when laminin was selectively immobilized onto mPEG rhNtA-SAMs (Fig. 5B, left panel). Data from image quantitative analysis (Fig. 5C–F) support this observation, as a higher tendency for the formation of larger polygonal-based (Fig. 5C–E) and organized (Fig. 5F) structures is evident as result of laminin polymerization. Moreover, the formed homogeneous matrix presents a fractal-like organization (Fig. 5B, left panel) and resembles

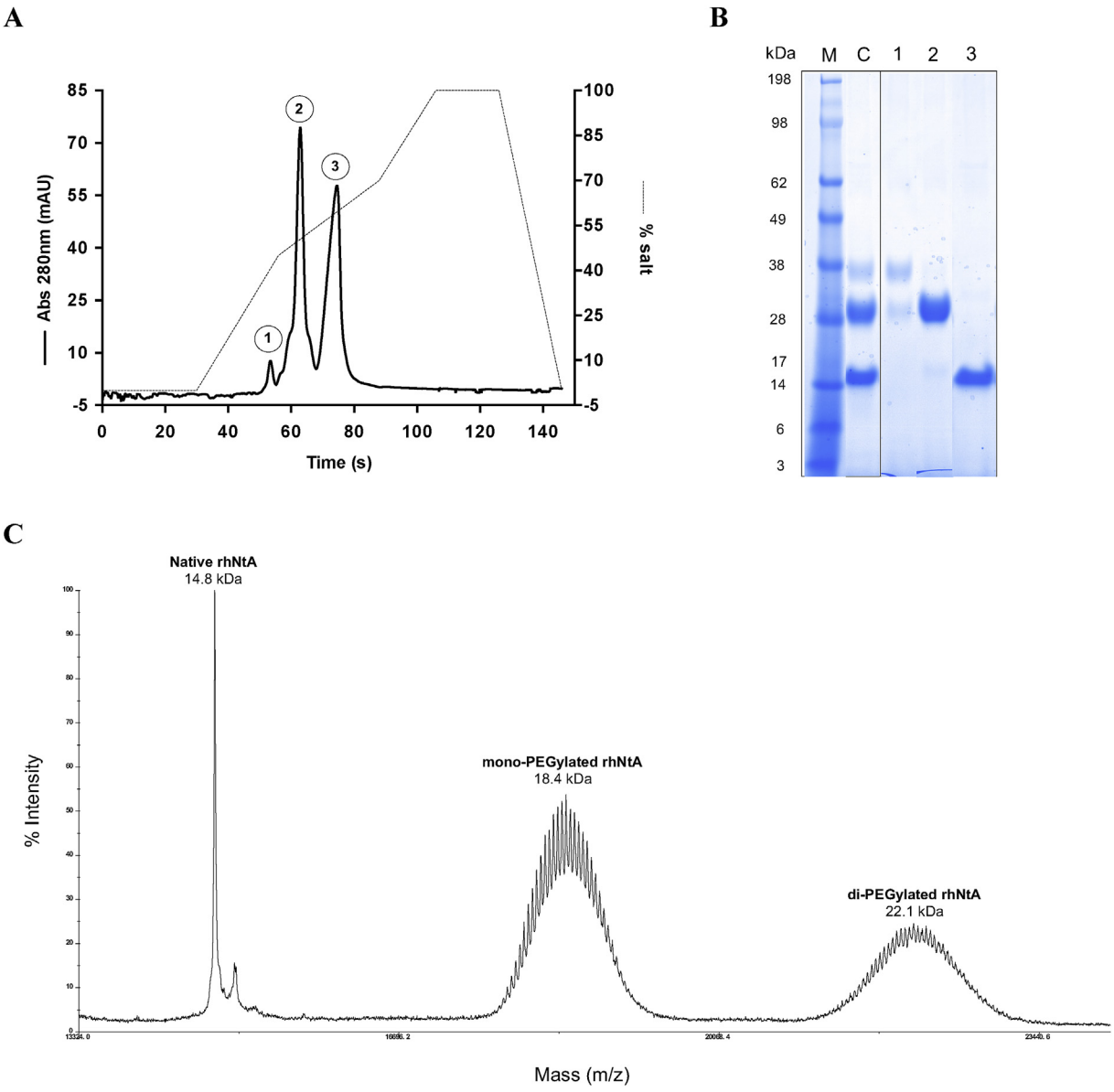


**Fig. 4. Characterization of N-terminal PEGylated rhNtA. A)** Cation-exchange chromatogram of the conjugation mixture. The chromatogram was obtained by monitoring the eluent at 280 nm and using a HiTrap SP HP column (GE Healthcare); 1, di-PEGylated rhNtA; 2, mono-PEGylated rhNtA; 3, Native rhNtA. **B)** Coomassie Blue stained 4–12% Bis-Tris gel of native and PEGylated rhNtA after purification. M, MW marker; C, Conjugation mixture before cation-exchange chromatography; 1, di-PEGylated rhNtA band at around 36.5 kDa; 2, mono-PEGylated rhNtA band at around 28.8 kDa; 3, native rhNtA at around 14.9 kDa. **C)** MALDI-TOF MS spectra of native and PEGylated rhNtA. The presented molecular weight corresponds to the value obtained for the high intensity peak – Native rhNtA 14.8 kDa; mono-PEGylated rhNtA 18.4 kDa; di-PEGylated rhNtA 22.1 kDa.

**Table 2**
Kinetic parameters ($k_a$ and $k_d$) and affinity constant ($K_D$) of mono-PEGylated rhNtA to immobilized msLn-111 or rhLn-521, estimated by SPR. Data represent mean ± SD of three independent experiments.

| | $k_a$ (x$10^5$) $M^{-1}.s^{-1}$ | $k_d$ (x$10^{-4}$) $s^{-1}$ | $K_D$ (nM) |
|---|---|---|---|
| **msLn-111** | 1.38 ± 0.05 | 4.64 ± 0.31 | 3.36 ± 0.11 |
| **rhLn-521** | 1.66 ± 0.63 | 2.47 ± 0.40 | 1.58 ± 0.41 |

the pattern of the networks reported in literature [42,54,55]. On the other hand, the non-selective covalent immobilization of laminin onto SGA-SAMs, led to the formation of a matrix consisting mainly of several smaller aggregates (Fig. 5C–E), which are extended over several focal plans with no observable formation of polygon-based structures (Fig. 5B, right panel). The inability to form a more organized structure is evidenced by the lower values of maximum Feret's diameter (Fig. 5F). The 3D structures of the different formed laminin matrices can be better appreciated in the animation movies presented as Movie S1–S2 in Supporting Information. The combination of the three independent variables (aggregate average size, perimeter and maximum Feret's diameter) and its analysis using the Fisher's combined probability test [56], also revealed statistically significant differences ($p < 0.0001$) on laminin self-polymerization between mPEG rhNtA- and SGA-SAMs. Overall, the results obtained showed that depending on the binding ligand (mono-PEGylated rhNtA *vs.* HS-PEG-SGA), structural distinct matrices can be formed. Moreover, we demonstrate that only when we promote the site-selective immobilization of laminin (mPEG rhNtA-SAMs), one retains its natural/intrinsic ability to self-polymerize.

Supplementary data related to this article can be found online at https://doi.org/10.1016/j.biomaterials.2018.10.039.

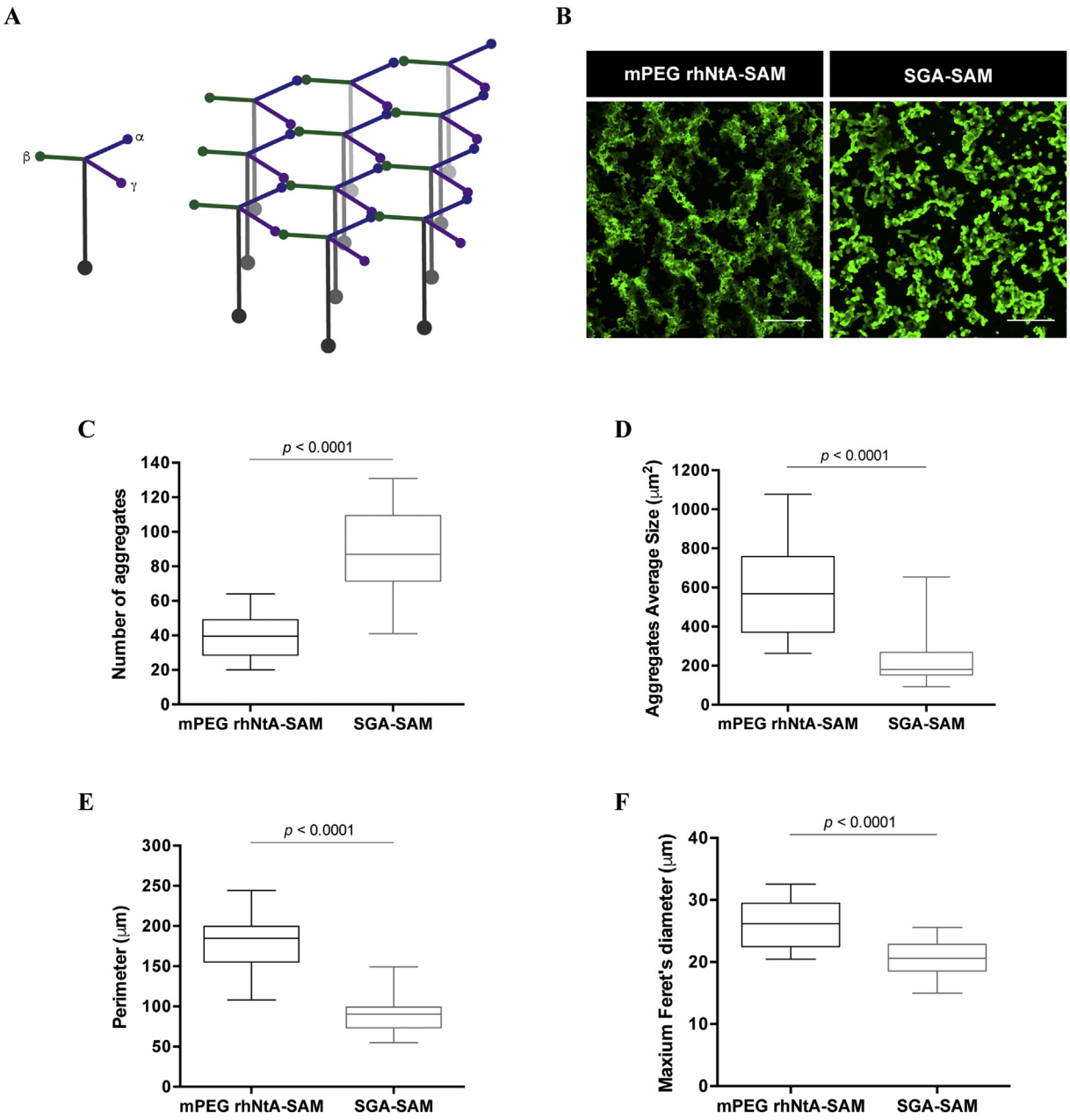


**Fig. 5. Assessment of the ability of site-selective immobilized laminin to self-polymerize**. **A)** Schematic representation of laminin self-polymerization (not to scale). Adapted from [57]. N-terminal domains of α, β and γ chains interact to form a polygonal network. The long arm is not involved in the network formation. **B)** mPEG rhNtA-SAM (left panel) or SGA-SAM (right panel) were incubated with msLn-111 (50 μg/mL) for 24 h, under neutral conditions (pH 7.0), and samples processed for immunofluorescence staining of laminin. Scale Bar = 50 μm. **C)** Number of aggregates; **D)** Aggregate average size (μm$^2$); **E)** Perimeter (μm); and **F)** Maximum Feret's diameter (μm) determined by image processing and quantitative analysis using ImageJ/Fiji and MATLAB® software, respectively. Data represent median and interquartile range (IQR) of 13–16 replicate samples from three independent assays; Mann-Whitney *U* test.

*3.5.2. Site-selective immobilized rhLn-521 support hNSC adhesion and spreading*

rhLn-521 has a key role in the modulation of neural cell behavior, including neuronal adhesion, viability and network formation [36,58]. Indeed, several studies have shown the potential of this laminin isoform to be used as a robust substratum for the culture and renewal of human embryonic [59] and pluripotent [36] stem cells. With this in mind, to assess laminin ability to mediate hNSC adhesion and spreading upon its binding to mPEG rhNtA-SAMs, rhLn-521 was used. QCM-D analysis was first conducted to follow the kinetics of rhLn-521 immobilization onto SAMs (Fig. 6A and B). Then, to characterize whether the proposed strategy favored the exposure of rhLn-521 cell-adhesive domains, hNSC adhesion and spreading was assessed (Fig. 6C–E).

QCM-D monitoring of rhLn-521 immobilization onto mPEG rhNtA-SAMs indicated a protein immobilization (638 ± 29 ng/cm$^2$, Fig. 6B), with mass per surface area values close to the theoretical value calculated for laminin immobilization under these conditions (952 ng/cm$^2$). This suggests that the immobilized mono-PEGylated rhNtA retained a 3D conformation that allowed the selective interaction with laminin. Moreover, mPEG rhNtA SAMs led to an immobilization degree statistically similar to that observed for uncoated Au surfaces (1130 ± 348 ng/cm$^2$), in which laminin may randomly adsorb over the entire surface. SGA-SAMs, in contrast, presented lower amounts of immobilized rhLn-521 (342 ± 44 ng/cm$^2$) (Fig. 6B), when compared to mPEG rhNtA-SAMs. As HS-PEG-SGA moieties can randomly interact with different amine groups within a single laminin molecule, these

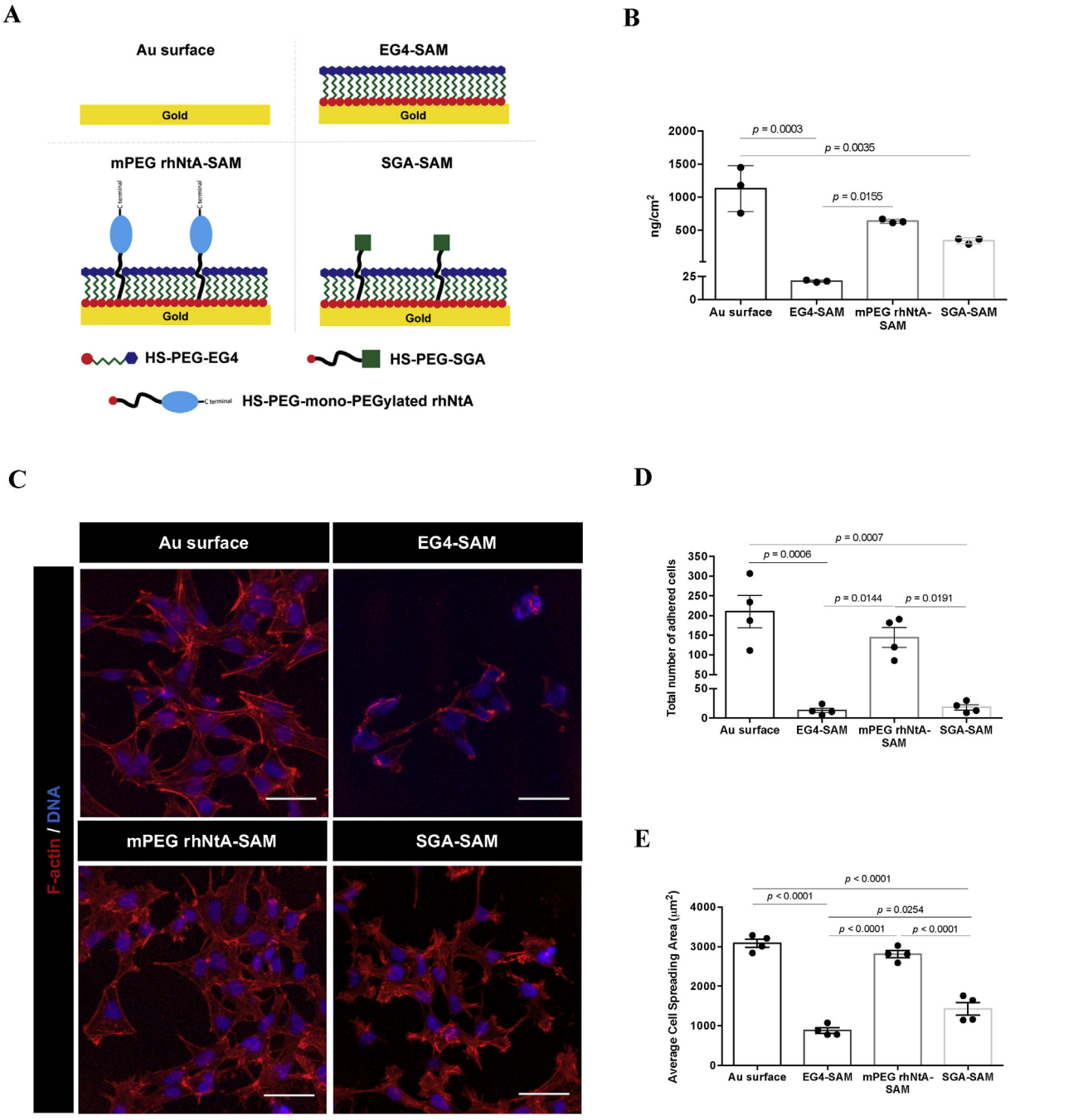


**Fig. 6. Immobilization of rhLn-521 onto SAMs and its effect on hNSC adhesion and spreading. A)** Schematic representation of the prepared surfaces (not to scale) – Au surface (control surface), EG4-SAM (non-fouling surface), mPEG rhNtA-SAM (for site-selective immobilization of laminin) and SGA-SAM (for non-selective covalent immobilization of laminin). **B)** QCM-D analysis of rhLn-521 immobilization (ng/cm$^2$) on SAMs. Data represent mean ± SD of three independent experiments; one-way ANOVA followed by Bonferroni's test. **C)** Representative 2D projections of CLSM 3D stack images of adhered hNSCs, after 24 h of culture. Scale Bar = 50 μm; **D)** Total number of adherent cells; and **E)** Average cell spreading area (μm$^2$) determined by quantitative analysis of images acquired with an IN Cell Analyzer 2000 imaging system. Data represent mean ± standard error of the mean (SEM) of four replicate samples from an experiment representative of three independent assays; one-way ANOVA followed by Bonferroni's test.

results suggest that the conformation of covalently-bound laminin and its spatial arrangement at the surface were distinct from that of affinity-bound laminin, leaving less area for the immobilization of other laminin molecules. As expected, the amount of adsorbed rhLn-521 on EG4-SAMs, was very low (20 ± 1 ng/cm$^2$) (Fig. 6B).

Site-selective immobilization of laminin onto mPEG rhNtA-SAMs led to hNSC adhesion comparable to that observed on rhLn-521-coated Au surfaces, used here as a control surface for hNSC adhesion (Fig. 6D and S8). After 24 h of culture, cells were well-spread (Fig. 6E and S9), exhibiting a morphology (Fig. 6C) comparable to that observed for cells seeded on rhLn-521-coated Au surfaces (Fig. 6C). Moreover, cells adhered to mPEG rhNtA-SAMs exhibit an average spreading area of 2812 ± 89 μm$^2$ (Fig. 6E), comparable to that observed for cells cultured on rhLn-521-coated Au surfaces (3089 ± 101 μm$^2$; Fig. 6E). TCPS surfaces, which are conventional used in adhesion studies, were used herein as additional control surfaces. The morphology of cells seeded on rhLn-521- site-selective immobilized on SAMs or -coated on Au surfaces is comparable to that observed on rhLn-521-modified TCPS

surfaces (Fig. S7). In addition, the average cell spreading area in these conditions is similar to that observed in TCPS surfaces (3496 ± 483 $\mu m^2$). The non-selective immobilization of laminin onto SGA-SAMs, in turn, resulted in a significantly lower cell adhesion ($p = 0.0191$; Fig. 6D and S8) and average spreading area (1430 ± 161 $\mu m^2$; $p < 0.0001$; Fig. 6E and S9) when compared to mPEG rhNtA-SAMs. Moreover, cells with both spread (Fig. 6C) and round (Fig. S7) morphology were observed. These results suggest that the non-selective nature of the immobilization process partially compromises the exposure of laminin cell binding domains, despite the considerable amount of rhLn-521 bound to SGA-SAMs (342.3 ± 43.6 $ng/cm^2$) (Fig. 6B). As expected, on EG4-SAMs, the few adherent cells (Fig. 6D and S8) presented mainly a round morphology (Fig. 6C and S7), as evidenced by the low average cell spreading area (881 ± 70 $\mu m^2$, Fig. 6E). Overall, these results clearly demonstrate that site-specific immobilization of laminin through the use of mono-PEGylated rhNtA better preserved laminin bioactivity in terms of ability to self-polymerize and to mediate hNSC adhesion and spreading, when compared to non-selective covalent immobilization approaches.

## 4. Conclusion

The present work demonstrates the potential of mono-PEGylated rhNtA as an effective natural affinity binding ligand for site-selective immobilization of laminin, allowing the preservation of laminin ability to self-polymerize and mediate cell adhesion and spreading. This affinity binding strategy overcomes several drawbacks associated with the currently available strategies for laminin immobilization. Moreover, this approach is highly versatile, as result of the ability of NtA to bind the different laminin isoforms that comprise the γ1 chain, which represent more than 50% of the isoforms identified to date [60], with variations in affinity imposed by α and β chains. Therefore, this strategy enables the immobilization of different laminin isoforms, which can be of interest for particular cell types and for application in specific disease contexts. Overall, the proposed strategy is highly attractive for a broad range of applications, including 2D coatings for cell culture, functionalization of 3D matrices for cell and/or drug delivery, engineered coatings for neuroelectrodes, among others.

## Conflicts of interest

The authors declare no conflicts of interest.

## Data availability

The raw/processed data generated and/or analyzed during the current study are available from the corresponding author on request.

## Acknowledgments

The mass spectrometry technique was performed at the Proteomics i3S Scientific Platform (Roteiro/0028/2013; LISBOA-01-0145-FEDER-022125) with the assistance of Hugo Osório. IRRAS analysis was performed at the Biointerfaces and Nanotechnology Scientific Platform, with the assistance of Ricardo Vidal. In Cell Analyzer experiments were performed at the Biosciences Screening i3S Scientific Platform, member of the PPBI (PPBI-POCI-01-0145-FEDER-022122) with the assistance of André Maia. Confocal microscopy was conducted at the Bioimaging i3S Scientific Platform, member of the PPBI (PPBI-POCI-01-0145-FEDER-022122), with the assistance of Maria Lázaro. This work was supported by projects NORTE-01-0145-FEDER-000008 and NORTE-01-0145-FEDER-000012, supported by Norte Portugal Regional Operational Programme (NORTE 2020), under the PORTUGAL 2020 Partnership Agreement, through the European Regional Development Fund (ERDF) and FEDER - Fundo Europeu de Desenvolvimento Regional funds through the COMPETE 2020 - Operational Programme for Competitiveness and Internationalisation (POCI), Portugal 2020; by Portuguese funds through FCT/MCTES in the framework of the project "Institute for Research and Innovation in Health Sciences" (POCI-01-0145-FEDER-007274) and by project COMBINE (Santa Casa da Misericordia de Lisboa – Prémio Neurociências Mello e Castro).

D.B. was supported by FCT PhD Programs (PD/BD/105953/2014) and Programa Operacional Potencial Humano (POCH), in the scope of the BiotechHealth Program (Doctoral Program on Cellular and Molecular Biotechnology Applied to Health Sciences), Programa FLAD Helthcare 2020 and the project PARES (Prémio Albino Aroso). Eduardo Conde-Sousa was supported by a post-doctoral grant of the project PPBI-POCI-01-0145-FEDER-022122, in the scope of Fundação para a Ciência e Tecnologia, Portugal (FCT) National Roadmap of Research Infrastructures.

## Appendix A. Supplementary data

Supplementary data to this article can be found online at https://doi.org/10.1016/j.biomaterials.2018.10.039.

## References

[1] J.H. Miner, B.L. Patton, S.I. Lentz, D.J. Gilbert, W.D. Snider, N.A. Jenkins, N.G. Copeland, J.R. Sanes, The laminin alpha chains: expression, developmental transitions, and chromosomal locations of alpha1-5, identification of heterotrimeric laminins 8-11, and cloning of a novel alpha 3 isoform, J. Cell Biol. 137 (3) (1997) 685–701.
[2] M. Falk, M. Ferletta, E. Forsberg, P. Ekblom, Restricted distribution of laminin alpha1 chain in normal adult mouse tissues, Matrix Biol. 18 (6) (1999) 557–568.
[3] H. Colognato, P.D. Yurchenco, Form and function: the laminin family of heterotrimers, Dev. Dynam. 218 (2) (2000) 213–234.
[4] T. Sasaki, R. Giltay, U. Talts, R. Timpl, J.F. Talts, Expression and distribution of laminin alpha1 and alpha 2 chains in embryonic and adult mouse tissues: an immunochemical approach, Exp. Cell Res. 275 (2) (2002) 185–199.
[5] J. Tzu, M.P. Marinkovich, Bridging structure with function: structural, regulatory, and developmental role of laminins, Int. J. Biochem. Cell Biol. 40 (2) (2008) 199–214.
[6] P.D. Yurchenco, E.C. Tsilibary, A.S. Charonis, H. Furthmayr, Laminin polymerization in vitro. Evidence for a two-step assembly with domain specificity, J. Biol. Chem. 260 (12) (1985) 7636–7644.
[7] P.D. Yurchenco, Y.S. Cheng, Self-assembly and calcium-binding sites in laminin. A three-arm interaction model, J. Biol. Chem. 268 (23) (1993) 17286–17299.
[8] Y.S. Cheng, M.F. Champliaud, R.E. Burgeson, M.P. Marinkovich, P.D. Yurchenco, Self-assembly of laminin isoforms, J. Biol. Chem. 272 (50) (1997) 31525–31532.
[9] J.D. Lathia, B. Patton, D.M. Eckley, T. Magnus, M.R. Mughal, T. Sasaki, M.A. Caldwell, M.S. Rao, M.P. Mattson, C. ffrench-Constant, Patterns of laminins and integrins in the embryonic ventricular zone of the CNS, J. Comp. Neurol. 505 (6) (2007) 630–643.
[10] K.J. Hamill, K. Kligys, S.B. Hopkinson, J.C. Jones, Laminin deposition in the extracellular matrix: a complex picture emerges, J. Cell Sci. 122 (Pt 24) (2009) 4409–4417.
[11] M. Aumailley, The laminin family, Cell Adhes. Migrat. 7 (1) (2013) 48–55.
[12] A.C. Taylor, C.H. Gonzalez, B.S. Miller, R.J. Edgington, P. Ferretti, R.B. Jackman, Surface functionalisation of nanodiamonds for human neural stem cell adhesion and proliferation, Sci. Rep. 7 (1) (2017) 7307.
[13] S.E. Stabenfeldt, A.J. Garcia, M.C. LaPlaca, Thermoreversible laminin-functionalized hydrogel for neural tissue engineering, J. Biomed. Mater. Res. 77 (4) (2006) 718–725.
[14] S.E. Stabenfeldt, G. Munglani, A.J. Garcia, M.C. LaPlaca, Biomimetic microenvironment modulates neural stem cell survival, migration, and differentiation, Tissue Eng. 16 (12) (2010) 3747–3758.
[15] S.E. Stabenfeldt, M.C. LaPlaca, Variations in rigidity and ligand density influence neuronal response in methylcellulose-laminin hydrogels, Acta Biomater. 7 (12) (2011) 4102–4108.
[16] A.T. Francisco, R.J. Mancino, R.D. Bowles, J.M. Brunger, D.M. Tainter, Y.T. Chen, W.J. Richardson, F. Guilak, L.A. Setton, Injectable laminin-functionalized hydrogel for nucleus pulposus regeneration, Biomaterials 34 (30) (2013) 7381–7388.
[17] A.T. Francisco, P.Y. Hwang, C.G. Jeong, L. Jing, J. Chen, L.A. Setton, Photocrosslinkable laminin-functionalized polyethylene glycol hydrogel for intervertebral disc regeneration, Acta Biomater. 10 (3) (2014) 1102–1111.
[18] C.P. Addington, J.M. Heffernan, C.S. Millar-Haskell, E.W. Tucker, R.W. Sirianni, S.E. Stabenfeldt, Enhancing neural stem cell response to SDF-1alpha gradients through hyaluronic acid-laminin hydrogels, Biomaterials 72 (2015) 11–19.
[19] J. Arulmoli, H.J. Wright, D.T.T. Phan, U. Sheth, R.A. Que, G.A. Botten, M. Keating, E.L. Botvinick, M.M. Pathak, T.I. Zarembinski, D.S. Yanni, O.V. Razorenova, C.C.W. Hughes, L.A. Flanagan, Combination scaffolds of salmon fibrin, hyaluronic acid, and laminin for human neural stem cell and vascular tissue engineering, Acta Biomater. 43 (2016) 122–138.
[20] C.P. Addington, S. Dharmawaj, J.M. Heffernan, R.W. Sirianni, S.E. Stabenfeldt,

Hyaluronic acid-laminin hydrogels increase neural stem cell transplant retention and migratory response to SDF-1alpha, Matrix Biol. 60–61 (2017) 206–216.
[21] B.G. Keselowsky, D.M. Collard, A.J. Garcia, Surface chemistry modulates fibronectin conformation and directs integrin binding and specificity to control cell adhesion, J. Biomed. Mater. Res. 66 (2) (2003) 247–259.
[22] J.C. Rodriguez Hernandez, M. Salmeron Sanchez, J.M. Soria, J.L. Gomez Ribelles, M. Monleon Pradas, Substrate chemistry-dependent conformations of single laminin molecules on polymer surfaces are revealed by the phase signal of atomic force microscopy, Biophys. J. 93 (1) (2007) 202–207.
[23] O.M. Ba, M. Hindie, P. Marmey, O. Gallet, K. Anselme, A. Ponche, A.C. Duncan, Protein covalent immobilization via its scarce thiol versus abundant amine groups: effect on orientation, cell binding domain exposure and conformational lability, Colloids Surfaces B Biointerfaces 134 (2015) 73–80.
[24] C.D. Spicer, B.G. Davis, Selective chemical protein modification, Nat. Commun. 5 (2014) 4740.
[25] O. Boutureira, G.J. Bernardes, Advances in chemical protein modification, Chem. Rev. 115 (5) (2015) 2174–2195.
[26] S.A. Fisher, A.E.G. Baker, M.S. Shoichet, Designing peptide and protein modified hydrogels: selecting the optimal conjugation strategy, J. Am. Chem. Soc. 139 (22) (2017) 7416–7427.
[27] J.P. Lee, E. Kassianidou, J.I. MacDonald, M.B. Francis, S. Kumar, N-terminal specific conjugation of extracellular matrix proteins to 2-pyridinecarboxaldehyde functionalized polyacrylamide hydrogels, Biomaterials 102 (2016) 268–276.
[28] C.C. Lin, K.S. Anseth, Controlling affinity binding with peptide-functionalized poly (ethylene glycol) hydrogels, Adv. Funct. Mater. 19 (14) (2009) 2325.
[29] J. Parker, N. Mitrousis, M.S. Shoichet, Hydrogel for simultaneous tunable growth factor delivery and enhanced viability of encapsulated cells in vitro, Biomacromolecules 17 (2) (2016) 476–484.
[30] S.E. Sakiyama-Elbert, J.A. Hubbell, Controlled release of nerve growth factor from a heparin-containing fibrin-based cell ingrowth matrix, J. Contr. Release 69 (1) (2000) 149–158.
[31] S.E. Sakiyama-Elbert, J.A. Hubbell, Development of fibrin derivatives for controlled release of heparin-binding growth factors, J. Contr. Release 65 (3) (2000) 389–402.
[32] J.B. Mascarenhas, M.A. Ruegg, U. Winzen, W. Halfter, J. Engel, J. Stetefeld, Mapping of the laminin-binding site of the N-terminal agrin domain (NtA), EMBO J. 22 (3) (2003) 529–536.
[33] A.J. Denzer, T. Schulthess, C. Fauser, B. Schumacher, R.A. Kammerer, J. Engel, M.A. Ruegg, Electron microscopic structure of agrin and mapping of its binding site in laminin-1, EMBO J. 17 (2) (1998) 335–343.
[34] R.A. Kammerer, T. Schulthess, R. Landwehr, B. Schumacher, A. Lustig, P.D. Yurchenco, M.A. Ruegg, J. Engel, A.J. Denzer, Interaction of agrin with laminin requires a coiled-coil conformation of the agrin-binding site within the laminin gamma 1 chain, EMBO J. 18 (23) (1999) 6762–6770.
[35] G.A. Hudalla, W.L. Murphy, Chemically well-defined self-assembled monolayers for cell culture: toward mimicking the natural ECM, Soft Matter 7 (20) (2011) 9561–9571.
[36] A. Hyysalo, M. Ristola, M.E. Makinen, S. Hayrynen, M. Nykter, S. Narkilahti, Laminin alpha 5 substrates promote survival, network formation and functional development of human pluripotent stem cell-derived neurons in vitro, Stem Cell Res. 24 (2017) 118–127.
[37] J. Scholz, H. Besir, C. Strasser, S. Suppmann, A new method to customize protein expression vectors for fast, efficient and background free parallel cloning, BMC Biotechnol. 13 (2013) 12.
[38] C.D. Reyes, A.J. Garcia, A centrifugation cell adhesion assay for high-throughput screening of biomaterial surfaces, J. Biomed. Mater. Res. 67 (1) (2003) 328–333.
[39] C. Gomes, A. Almeida, J.A. Ferreira, L. Silva, H. Santos-Sousa, J. Pinto-de-Sousa, L.L. Santos, F. Amado, T. Schwientek, S.B. Levery, U. Mandel, H. Clausen, L. David, C.A. Reis, H. Osorio, Glycoproteomic analysis of serum from patients with gastric precancerous lesions, J. Proteome Res. 12 (3) (2013) 1454–1466.
[40] P. Parreira, A. Magalhaes, I.C. Goncalves, J. Gomes, R. Vidal, C.A. Reis, D.E. Leckband, M.C. Martins, Effect of surface chemistry on bacterial adhesion, viability, and morphology, J. Biomed. Mater. Res. 99 (3) (2011) 344–353.
[41] F. Costa, D.M. Sousa, P. Parreira, M. Lamghari, P. Gomes, M.C.L. Martins, N-acetylcysteine-functionalized coating avoids bacterial adhesion and biofilm formation, Sci. Rep. 7 (1) (2017) 17374.
[42] E. Freire, F.C. Gomes, R. Linden, V.M. Neto, T. Coelho-Sampaio, Structure of laminin substrate modulates cellular signaling for neuritogenesis, J. Cell Sci. 115 (Pt 24) (2002) 4867–4876.
[43] A.E. Carpenter, T.R. Jones, M.R. Lamprecht, C. Clarke, I.H. Kang, O. Friman, D.A. Guertin, J.H. Chang, R.A. Lindquist, J. Moffat, P. Golland, D.M. Sabatini, CellProfiler: image analysis software for identifying and quantifying cell phenotypes, Genome Biol. 7 (10) (2006) R100.
[44] J. Stetefeld, M. Jenny, T. Schulthess, R. Landwehr, B. Schumacher, S. Frank, M.A. Ruegg, J. Engel, R.A. Kammerer, The laminin-binding domain of agrin is structurally related to N-TIMP-1, Nat. Struct. Biol. 8 (8) (2001) 705–709.
[45] M.C. Tate, A.J. Garcia, B.G. Keselowsky, M.A. Schumm, D.R. Archer, M.C. LaPlaca, Specific beta 1 integrins mediate adhesion, migration, and differentiation of neural progenitors derived from the embryonic striatum, Mol. Cell. Neurosci. 27 (1) (2004) 22–31.
[46] L.A. Flanagan, L.M. Rebaza, S. Derzic, P.H. Schwartz, E.S. Monuki, Regulation of human neural precursor cells by laminin and integrins, J. Neurosci. Res. 83 (5) (2006) 845–856.
[47] J. Silva, A.R. Bento, D. Barros, T.L. Laundos, S.R. Sousa, P. Quelhas, M.M. Sousa, A.P. Pego, I.F. Amaral, Fibrin functionalization with synthetic adhesive ligands interacting with alpha6beta 1 integrin receptor enhance neurite outgrowth of embryonic stem cell-derived neural stem/progenitors, Acta Biomater. 59 (2017) 243–256.
[48] S.L. Hirsh, D.R. McKenzie, N.J. Nosworthy, J.A. Denman, O.U. Sezerman, M.M. Bilek, The Vroman effect: competitive protein exchange with dynamic multilayer protein aggregates, Colloids Surfaces B Biointerfaces 103 (2013) 395–404.
[49] O. Kinstler, G. Molineux, M. Treuheit, D. Ladd, C. Gegg, Mono-N-terminal poly (ethylene glycol)-protein conjugates, Adv. Drug Deliv. Rev. 54 (4) (2002) 477–485.
[50] J. Wang, T. Hu, Y. Liu, G. Zhang, G. Ma, Z. Su, Kinetic and stoichiometric analysis of the modification process for N-terminal PEGylation of staphylokinase, Anal. Biochem. 412 (1) (2011) 114–116.
[51] A.J. Denzer, R. Brandenberger, M. Gesemann, M. Chiquet, M.A. Ruegg, Agrin binds to the nerve-muscle basal lamina via laminin, J. Cell Biol. 137 (3) (1997) 671–683.
[52] P. Parreira, A. Magalhaes, C.A. Reis, T. Boren, D. Leckband, M.C. Martins, Bioengineered surfaces promote specific protein-glycan mediated binding of the gastric pathogen Helicobacter pylori, Acta Biomater. 9 (11) (2013) 8885–8893.
[53] K.K. McKee, D. Harrison, S. Capizzi, P.D. Yurchenco, Role of laminin terminal globular domains in basement membrane assembly, J. Biol. Chem. 282 (29) (2007) 21437–21447.
[54] H. Colognato, D.A. Winkelmann, P.D. Yurchenco, Laminin polymerization induces a receptor-cytoskeleton network, J. Cell Biol. 145 (3) (1999) 619–631.
[55] C. Hochman-Mendez, M. Cantini, D. Moratal, M. Salmeron-Sanchez, T. Coelho-Sampaio, A fractal nature for polymerized laminin, PloS One 9 (10) (2014) e109388.
[56] R.R. Sokal, F.J. Rohlf, Biometry: the Principles and Practices of Statistics in Biological Research, W.H. Freeman and Company, 1994.
[57] E. Hohenester, P.D. Yurchenco, Laminins in basement membrane assembly, Cell Adhes. Migrat. 7 (1) (2013) 56–63.
[58] A. Bergeron, H. Sherman, P. Pardo, H. Gitschier, H. Nandivada, D. Saxena, Corning® RLaminin-521 (Human) for Expansion and Differentiation of Human Neural Stem Cells, Corning Incorporated | Application Note, 2015.
[59] S. Rodin, L. Antonsson, C. Niaudet, O.E. Simonson, E. Salmela, E.M. Hansson, A. Domogatskaya, Z. Xiao, P. Damdimopoulou, M. Sheikhi, J. Inzunza, A.S. Nilsson, D. Baker, R. Kuiper, Y. Sun, E. Blennow, M. Nordenskjold, K.H. Grinnemo, J. Kere, C. Betsholtz, O. Hovatta, K. Tryggvason, Clonal culturing of human embryonic stem cells on laminin-521/E-cadherin matrix in defined and xeno-free environment, Nat. Commun. 5 (2014) 3195.
[60] M. Aumailley, L. Bruckner-Tuderman, W.G. Carter, R. Deutzmann, D. Edgar, P. Ekblom, J. Engel, E. Engvall, E. Hohenester, J.C. Jones, H.K. Kleinman, M.P. Marinkovich, G.R. Martin, U. Mayer, G. Meneguzzi, J.H. Miner, K. Miyazaki, M. Patarroyo, M. Paulsson, V. Quaranta, J.R. Sanes, T. Sasaki, K. Sekiguchi, L.M. Sorokin, J.F. Talts, K. Tryggvason, J. Uitto, I. Virtanen, K. von der Mark, U.M. Wewer, Y. Yamada, P.D. Yurchenco, A simplified laminin nomenclature, Matrix Biol. 24 (5) (2005) 326–332.